Theoretical investigations of half-metallic ferromagnetism in new Half–Heusler YCrSb and YMnSb alloys using first-principle calculations

M Atif Sattar[1], Muhammad Rashid[2,†], M Raza Hashmi[1], S A Ahmad[1], Muhammad Imran[3], and Fayyaz Hussain[3]

[1] *Department of Physics Simulation Laboratory, the Islamia University of Bahawalpur,* 63100, *Pakistan*
[2] *Department of Physics, COMSATS Institute of Information Technology,* 44000 *Islamabad, Pakistan*
[3] *Department of Physics, Bahauddin Zakariya University, Multan* 60800, *Pakistan*

(Received 13 March 2016; revised manuscript received 21 May 2016; published online 25 September 2016)

Structural, electronic, and magnetic properties of new predicted half-Heusler YCrSb and YMnSb compounds within the ordered MgAgAs $C1_b$-type structure are investigated by employing first-principal calculations based on density functional theory. Through the calculated total energies of three possible atomic placements, we find the most stable structures regarding YCrSb and YMnSb materials, where Y, Cr(Mn), and Sb atoms occupy the (0.5, 0.5, 0.5), (0.25, 0.25, 0.25), and (0, 0, 0) positions, respectively. Furthermore, structural properties are explored for the non-magnetic and ferromagnetic and anti-ferromagnetic states and it is found that both materials prefer ferromagnetic states. The electronic band structure shows that YCrSb has a direct band gap of 0.78 eV while YMnSb has an indirect band gap of 0.40 eV in the majority spin channel. Our findings show that YCrSb and YMnSb materials exhibit half-metallic characteristics at their optimized lattice constants of 6.67 Å and 6.56 Å, respectively. The half-metallicities associated with YCrSb and YMnSb are found to be robust under large in-plane strains which make them potential contenders for spintronic applications.

Keywords: electronic structures, density functional theory, metals and alloys, other ferromagnetic metals and alloys

PACS: 74.25.Jb, 71.15.Mb, 75.20.En, 75.50.Cc **DOI:** 10.1088/1674-1056/25/10/107402

1. Introduction

To meet the essentials of the advance technological applications, the search for the best materials in general and for spintronics applications in particular is a challenge. Spin-polarized ferromagnetic materials are generally supposed to be the best replacements for conventional materials.[1] The quest for brand-new materials in the field of spintronics has guided towards Heusler alloys in the last three decades due to their ability to be strong candidates for spin based electronic materials. The important part regarding spintronics is a way to obtain spin-polarized charge carriers. Half metallic ferromagnets (HMFs) are a type of brand new material because of their distinctive characters and tend to be probably the most essential components designed for spintronics.[2] HMFs have attracted considerable interest within last three decades due to their unique property of possessing a semi-conducting behavior in one spin direction with a narrow gap at the Fermi level (E_F) producing 100% polarization at the E_F and metallic behavior in other spin direction. HMFs will be appealing materials that can result in high performance applications in spintronics devices, as a source of spin-polarized charge carriers injected, such as spin-field effect transistor (FET), spin-light emitting diode (LED) along with tunneling devices.[3] HMFs with half-Heusler (HH) structure offer the great possibility of integrating magnetic devices into semiconductor technologies and potential applications in spintronics due to their structural resemblance to the zinc-blende phase and relatively high Curie temperature.

In 1983, de Groot *et al.*[4] initially predicted the Half-metallic (HM) ferromagnetism by exploring the band structure calculations of Mn-based materials in semi-Heusler NiMnSb, which is right now more successful to be synthesized experimentally with single crystalline nature.[5] Several studies relevant to HMFs are already expected theoretically and also many of HMFs are validated experimentally. Half-metallicity is located in Heusler compounds[5–10] and several other kinds of materials which include ferromagnetic metallic oxides,[11–14] nanostructures,[15] binary transition metal pnictides (chemical compounds) as well as chalcogenides acquiring zinc-blended and rock-salt structural arrangements.[16–20]

Numerous studies have already been conducted on these types of materials and plenty of them have become HMFs. But often experimental synthesis of these materials at the room temperature is difficult, as half-metallicity is lost due to very small HM energy gap (E_{HM}) and very large magnetic moments arises. Small half metallic gap and large magnetic moment means high stray field. E_{HM} would frequently vanishes in each of these HH materials when strain mismatch rises at the interface with traditional semiconductor. In addition, HM materials having a large magnetic moment are not really ideal for spin-

†Corresponding author. E-mail: rapakistana@yahoo.com, muhammad.rashid@comsats.edu.pk
© 2016 Chinese Physical Society and IOP Publishing Ltd

tronic practical applications, since the big magnetic moment indicates higher stray fields as well as large energy deficits. This particular deficiency inspires us to find brand new HM alloys that have modest magnetic moment and larger E_{HM}. The outcomes offered by this study might be helpful in understanding the applications of these HH materials in the arena of spintronics. Structural, electronic, and magnetic properties of HH YCrSb and YMnSb are explored in this study for the sake of their novel applications.

The rest of this paper is arranged as follows. In Section 2, the details of computational technique are elaborated. Within Section 3, the particular stableness, electronic and magnetic attributes are presented and discussed. Finally, various conclusions are presented in Section 4.

2. Computational details

To cope with the exchange and correlation potential, all computations are executed within density function theory (DFT) using the generalized gradient approximation (GGA) available as Perdew–Burke–Ernzerhof (PBE) functional.[21] A cycle of self-consistent scheme is performed to find out the structural and electronic properties of YCrSb and YMnSb HH materials by solving the Kohn–Sham equations.[22] through utilizing the full-potential linearized augmented plane wave method (FPLAPW)[23] as implemented within the WIEN2K simulation code.[24] A k-point mesh of $15 \times 15 \times 15$ is chosen for the calculations of these HH materials each with muffin-tin sphere radius of 2.5 a.u (atomic unit), for Y, Cr(Mn), and Sb atoms, respectively, and the value of $R_{MT} \times K_{max}$ is set to be 9. Expansion of site-centered potentials and densities is taken with the angular momentum up to $l_{max} = 10$. The particular Brillouin zone (BZ) integration is completed from the standard tetrahedron approach.[25] For the two consecutive computations, the actual convergence criterion in this self-consistent information with regard to ionic relaxations is 10^{-5} eV/unit cell.

3. Results and discussion

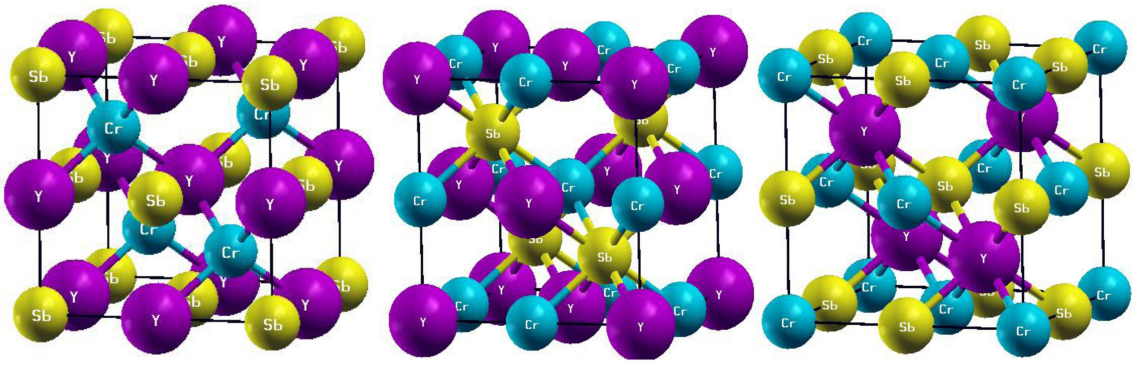
3.1. Structural arrangements and stability

HH alloy with general formula XYZ has only one magnetic sublattice, where X and Y are the transitional metals and Z is the main group element. HH materials belong to a family relating to traditional semiconductors such as Si or GaAs, and crystalize into non-centrosymmetric cubic MgAgAs–$C1_b$ structure (space group F-43m, No. 216) having 1:1:1 stoichiometry, which is ternary arranged different from the CaF_2 and can be derived from the tetrahedral ZnS-type structure.[26] The Wyckoff positions of the three interpenetrating fcc lattices are 4a (0, 0, 0), 4b (1/2, 1/2, 1/2), and 4c (1/4, 1/4, 1/4), and the 4d (3/4, 3/4, 3/4) site is empty. In essence X, Y, and Z atoms can occupy these Wyckoff positions 4a, 4b, and 4c sites, respectively. Three unique phases (X_I, X_{II}, X_{III}) are possible for X, Y, and Z atoms by changing these atomic positions in a unit cell, for instance X_I, X_{II}, and X_{III} phases can be organized at distinct Wyckoff positions.[27] Atomic layout for each phase is presented in Table 1. For an illustration, the crystal structures of YCrSb alloy for three possible atomic arrangements are shown in Fig. 1.

Table 1. Site preferences of X, Y, and Z atoms in three atomic arrangements X_I, X_{II}, and X_{III} in the $C1_b$ half-Heusler structure. The 4d site is empty.

Phase	4a (0, 0, 0)	4b (1/2, 1/2, 1/2)	4c (1/4, 1/4, 1/4)
X_I	Z	X	Y
X_{II}	X	Y	Z
X_{III}	Y	Z	X

Exploration of XYZ materials within three feasible arrangements is essential because a few experimental researches display that the composition associated with half-Heusler materials rely on the atomic disorderness.[27–29] The crystalline framework of $C1_b$-type structure associated with this kind of material can be reviewed properly from Refs. [30] and [31]. In our latest information, there is no experimental nor theoretical report so far, relating to both YCrSb and YMnSb HH materials. Murnaghan's equation of state[32] is utilized to find



X_I structure X_{II} structure X_{III} structure

Fig. 1. (color online) Conventional unit cells of YCrSb half-Heusler alloy in the MgAgAs ($C1_b$) structure for the three distinct X_I, X_{II}, and X_{III} atomic arrangements.

out the lattice constants. Prior to studying electronic and magnetic properties, stabilities of the crystal structure of YCrSb and YMnSb are checked by optimizing the total energy as a function of volume for all the three possible states. Variations of total energy with volumes of YCrSb and YMnSb compounds for all the three possible $X_{\rm I}$, $X_{\rm II}$, and $X_{\rm III}$ phases are shown in Fig. 2. It is obvious that $X_{\rm I}$ structures for the both compounds obtain the least minimized total energies compared with those of the other $X_{\rm II}$ and $X_{\rm III}$ feasible structures. Consequently, it is concluded that $X_{\rm I}$ structure is the most preferred phase because of its least minimized total energy and all further computations are performed at this specific ground state phase. The outcomes are ascribed to the following reasons: (i) within the $X_{\rm I}$ structure, Cr sorts the nearest neighbor (NN) surrounds with both Y and Sb, although Sb has both Cr and Y as NN pairs for the $X_{\rm II}$ structure; (ii) the size of Y is greater than that of Cr. Therefore, a strong bond is established between Cr and Y resulting in the minimum total energy in the $X_{\rm I}$ structure. In the $X_{\rm III}$ structure, Sb is not in the NN arrangement with Cr.

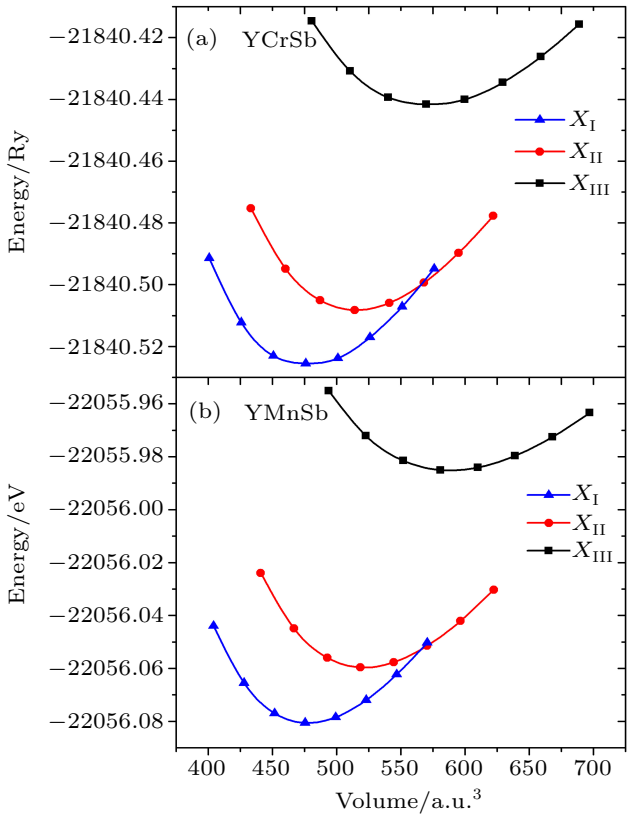


Fig. 2. (color online) Variations of computed ferromagnetictotal energy with volume per unit cell for the three feasible atomic arrangements $X_{\rm I}$, $X_{\rm II}$, and $X_{\rm III}$ of both half-Heusler (a) YCrSb and (b) YMnSb with MgAgAa ($C1_{\rm b}$) structure. The unit 1 Ry = 13.6056923(12) eV

The optimized lattice constants of the YCrSb and YMnSb HH materials for stable $X_{\rm I}$ phase are 6.673 Å and 6.565 Å, respectively. For these two studied compounds with the ferromagnetic state, the computed lattice constant, total energy, bulk modulus B (in unit GPa) and first order derivative of the modulus B' evaluated by using unit cell volume at zero pressure for the three unique phases are detailed in Table 2. As yet, neither experimental data for the bulk moduli nor the lattice constants of the studied compounds are available to be compared with the theoretical results.

Table 2. Values of Optimized lattice constant $a_{\rm opt}$ (in unit Å), the bulk modulus B (in unit GPa), the pressure derivative of the bulk modulus B, the total energy (in unit Ry) of the YCrSb and YMnSb materials.

Compound	Structure	$a_{\rm opt}$/Å	B/GPa	B'	$E_{\rm tot}$/Ry	Half-metallicity
YCrSb	$X_{\rm I}$	6.673	64.6	4.71	−21840.5260	Yes
	$X_{\rm II}$	6.839	57.8	4.44	−21840.5081	No
	$X_{\rm III}$	7.068	44.25	4.07	−21840.4419	No
YMnSb	$X_{\rm I}$	6.565	68.10	4.78	−22056.0804	Yes
	$X_{\rm II}$	6.760	60.86	4.61	−22056.059	No
	$X_{\rm III}$	7.038	42.33	4.20	−22055.9851	No

Spin-polarized (magnetic phase) and non-spin polarized (non-magnetic phase) calculations are also carried out for each of YCrSb and YMnSb compounds within the stable $X_{\rm I}$ structure. The variations of total energy with volume are presented in Fig. 3 respectively for the non-magnetic (NM), ferromagnetic (FM), and anti-ferromagnetic (AFM) states, which clearly indicate that ferromagnetic state is energetically more favorable than non-magnetic and anti-ferromagnetic states. Furthermore, the total energy difference between NM and FM phases ($\Delta E_{\rm FM\text{-}NM}$) with stable $X_{\rm I}$-structure is given in Table 3. As can be seen, the values of $\Delta E_{\rm FM\text{-}NM}$ are negative for both the studied compounds, implying that the FM phase of such materials is actually much more steady than NM phase. Therefore the next discussion provides the actual ferromagnetic phase.

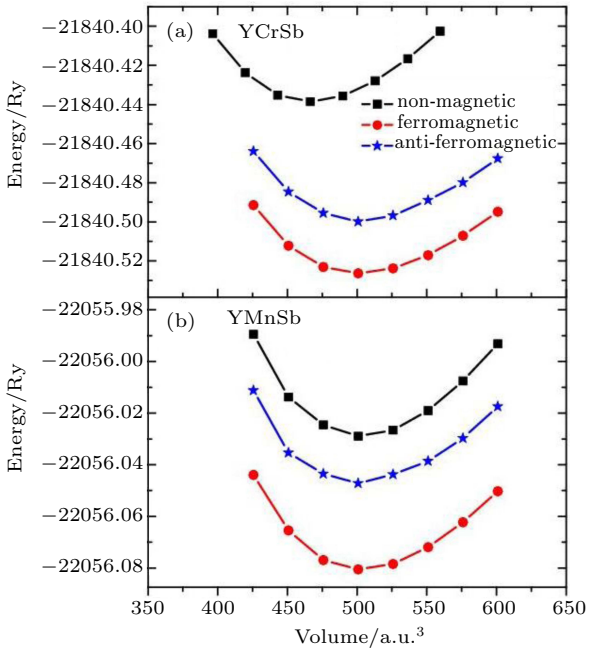


Fig. 3. (color online) Variations of calculated total energy with volume (a) YCrSb and (b) YMnSb in stable $X_{\rm I}$ phase for non-magnetic (NM), ferromagnetic (FM) and anti-ferromagnetic states.

Table 3. Calculated values of formation energy E_{for} (in unit eV) per formula unit, spin-up band gap E_g (in unit eV), half-metallic gap E_{HM} (in unit eV), and the energy difference between ferromagnetic and non-magnetic states $\Delta E_{FM\text{-}NM}$ (in unit eV) for YCrSb and YMnSb HH materials.

$(X)_{4a}$: $(Y)_{4b}$: $(Z)_{4c}$	E_g/eV	E_{HM}/eV	$\Delta E_{FM\text{-}NM}$/eV	E_{for}/eV	P/%
YCrSb	0.78	0.43	−1.68	−3.557	100
YMnSb	0.40	0.13	−1.19	−6.770	100

To confirm that the studied materials can possibly be synthesized experimentally, formation energy (ΔH_{for}) is also taken into consideration for the YCrSb and YMnSb materials which can be explained by using the following equation:

$$\Delta H_{for} = E_{YCr(Mn)Sb} - E_Y - E_{Cr(Mn)} - E_{Sb},$$

where $E_{YCr(Mn)Sb}$ is the total energy of the YCrSb and YMnSb materials calculated by the first principal calculations and E_Y, $E_{Cr(Mn)}$, E_{Sb} are energies of the corresponding individual atoms. Usually, negative formation energy signifies the stableness of the compound. Formation energies for the YCrSb and YMnSb HH materials are listed in Table 3. The lower value of formation energies for the studied compounds indicate that these materials can be synthesized experimentally.

3.2. Electronic properties

The electronic structure affects an essential part to identify the HM properties associated with HH materials. Band structures of YCrSb and YMnSb alloys are shown in Figs. 4 and 5, respectively. The left panel demonstrates the spin-up (majority) state, and the right panel indicates the bands for the spin-down (minority) state. The different colors in Fig. 4 represent different physical meaning. They show the contributions of s, p, and d orbitals of Y, Mn/Cr, and Sb atoms to electronic band structure. They reveal the information about which orbital of the atoms in the alloy is contributing more near the Fermi level and which atom orbital is in the core state. They also represent each eigenvalue along the k-path which we have previously selected during the SCF cycle.Obviously, it can be noted that half-metallicity has semiconducting gap (E_g) around the Fermi level (E_F) in the majority spin (spin-up) state (Figs. 4(a) and 5(a)), and that the band crosses the E_F and thus displays metallic nature in minority spin (spin-down) state (Figs. 4(b) and 5(b)). For both YCrSb and YMnSb HH materials in the majority spin channel, there are clear gaps E_g and E_{HM} in the majority band. The E_g is the energy band gap which is the spacing between the valance band maximum and the conduction band minimum, and the E_{HM} is the shortest distance twixt the most occupied valance band energy and the E_F. This particular parameter E_{HM} possess specific significance for the half metallicity of the ferromagnetic material rather than E_g along the E_F. The presence of non-zero flip gap (E_{HM}) for both the compounds in the majority spin channel indicates that they are true HMFs. The values of E_g, E_{HM}, and E_F calculated for both YCrSb and YMnSb HH materials are presented in Table 3. It can also be seen that the band transition for the YCrSb is direct (Γ–Γ) while an indirect band transition is found for the YMnSb (Γ–X) HH material. It can also be noted that bands near the E_F are triply degenerated at Γ for the majority spin channel.

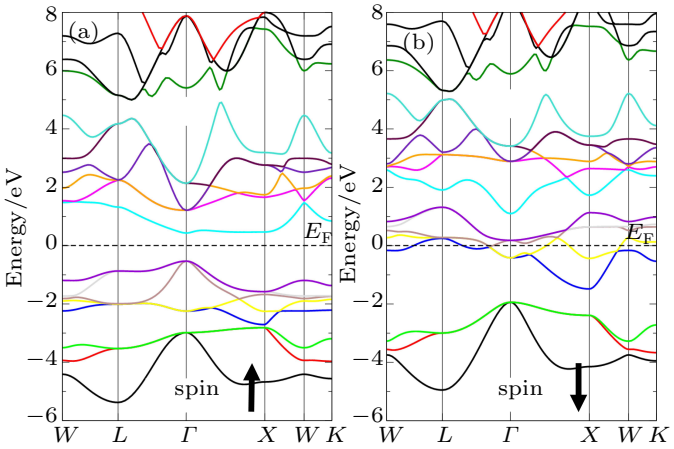


Fig. 4. (color online) Spin-resolved band structures of half-Heusler YCrSb (a) spin up and (b) spin down. Fermi level is set to be zero.

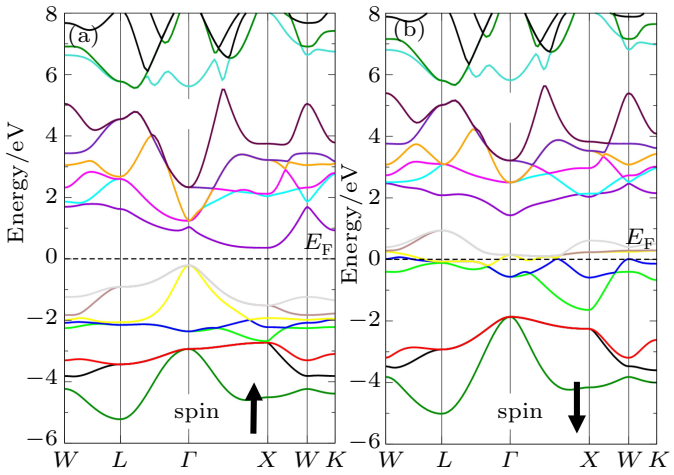


Fig. 5. (color online) Spin-resolved band structures of half-Heusler YMnSb (a) spin up and (b) spin down. Fermi level is set to zero.

The number of states for each period of energy which are occupied by the specific energy levels is usually explained by the density of states (DOS) of the system. To examine the electronic natures of the YCrSb and YMnSb materials, total and partial DOS within the magnetic phase designed for spin-up and spin-down channel are also measured by utilizing the PBE-GGA. The particular DOS graphics are displayed in Fig. 6 to analyze the E_g in the majority spin state of the studied materials at the equilibrium lattice constant. The spin-dependent total and orbital electronic DOS of YCrSb and YMnSb are presented in Fig. 6. Large spin splittings in these materials occur from Cr/Mn (d-t_{2g}) states with a small contribution from Y (d-t_{2g}) states. The contribution by the Sb atom near the E_F is quite small in comparison with the Cr/Mn (d-t_{2g}) and Y (d-t_{2g}) atoms. Also Sb atom has symmetrical state below the E_F having energy around −10 eV.

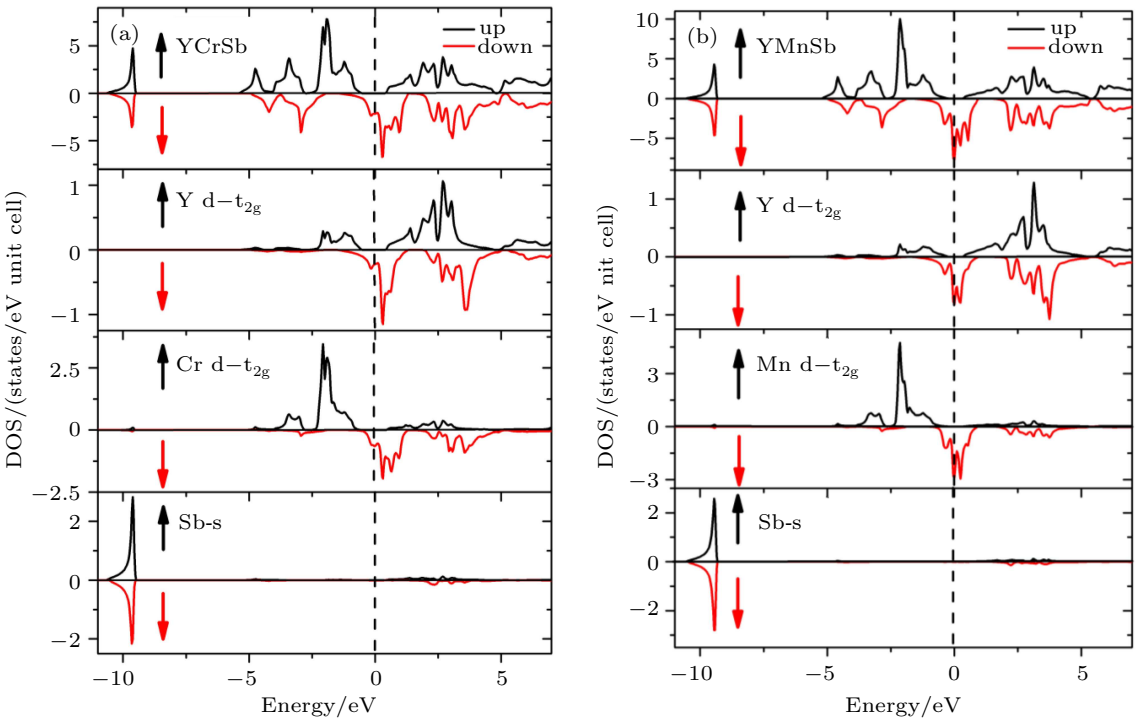


Fig. 6. (color online) Spin-polarized densities of state for the total and individual atoms at the equilibrium lattice constant for the X_I phase (a) YCrSb and (b) YMnSb.

A solid hybridization among the d-orbitals of Y, Cr, and Mn atoms is found, which divides the d orbitals of these atoms into d–e_g and d–t_{2g} states. A semiconducting gap is found for the majority-spin channel. It can be visualized that states near the E_F for both majority and minority spin states are mostly contributed due to the Cr/Mn (d–t_{2g}) and Y (d–t_{2g}) atoms, which is comparable to various other transition-metal element based HH materials.[3,33]

To clarify the origin of the semiconducting gap, d–d hybridization nearby the Fermi energy level can be revealed inside Fig. 7. Cr and Mn atoms are enclosed by Sb atoms, seeing them at NN and Y as next neighbor. Both Cr and Mn 3d states split up into the triplet associated with d–t_{2g} states and a doublet associated with e_g states because of the crystal field theory. In the majority spin channel, the d–t_{2g} and e_g states of Mn and Cr ought to be occupied in the minority spin states but electrons are depleted in the majority spin state due to the exchange interaction. These states turn out to be unoccupied and develop the semiconducting gap. Furthermore, the electronic spin-polarization at the E_F can be expressed by the following relation:[34]

$$P = \frac{\rho\uparrow(E_F) - \rho\downarrow(E_F)}{\rho\uparrow(E_F) + \rho\downarrow(E_F)},$$

where $\rho\uparrow(E_F)$ and $\rho\downarrow(E_F)$ are the densities of states at the E_F for the majority and minority spin states, respectively. The studied HH YCrSb and YMnSb materials have 100% spin-polarization (see Table 3), proving that electrons at the E_F are fully spin-polarized. That confirms the HM characteristics.

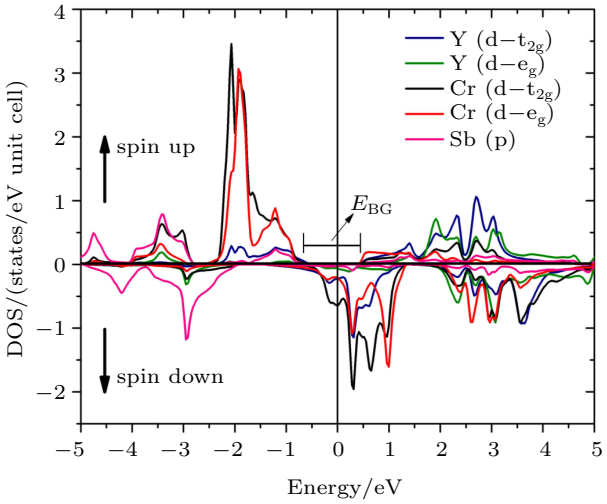


Fig. 7. (color online) Schematic representations of origin of semiconducting gap in the majority spin state in the stable X_I structure for the YCrSb.

3.3. Magnetic properties

The origin of magnetic moment for the HH alloy is described in this subsection. The total and individual magnetic moment of the atoms per unit cell in the unit of multiples of Bhor magnetron for the YCrSb and YMnSb for the X_I structural phase are presented in Table 4. The structures of HH materials can be decomposed right into a zinc blende (ZB) substructure along with variants within the occupancy from the interstitial lattice sites. There are three main mechanisms,[33] which govern the magnetic properties due to HM in the ZB structure: (i) the d-states of the Cr and Mn atoms (here it can even be Y-atom) split into triply (t_{2g}) and doubly (e_g) due

to the crystal field effect, (ii) bonding and antibonding states are formed when the sp^3-type state of Sb interacts with these triplet states, (iii) populations of the electrons change in the majority and minority spin channel due to the exchange interaction. The local magnetic moments of the crystal are formed by the remaining electrons of the Cr and Mn atoms. Due to the resemblance of HH alloy composition to the ZB structure, the magnetic moment arranged in Table 4 can be ascribed to the Mn and Cr atoms. As the HH materials contain only one magnetic sublattice consisting of the atoms on the octahedral sites,[26] which is also indicated in Table 4, the Cr and Mn atoms mainly contribute to the total magnetic moment for the studied HH materials and occupy the octahedral sites in the stable X_I structure. It can also be understood from the electronic arrangements. Electronic configurations for the Cr and Mn are $(3d)^5 4s$ and $(3d)^5 4(s)^2$, respectively. For pure metals, Cr and Mn, electronic spins form the magnetic moments according to the first Hund's rule but when these types of transition metals (Cr, Mn) are made into alloys, the availability of 3d-electrons will change because of diverse electro-negativity. In the stable X_I structure, Sb is the NN for the Cr and Mn in the HH YCrSb and YMnSb materials because of this a small charge is transferred from Cr and Mn to Sb by leaving lots of d-electrons at Cr and Mn atoms that govern the magnetic moments for these HH materials respectively.

Table 4. Calculated values of total and local magnetic moment (in unit μ_B) of the individual atom and interstitial site for YCrSb and YMnSb HH materials.

Compound	Y/μ_B	Cr/μ_B	Sb/μ_B	Interstitial/μ_B	Total/μ_B
YCrSb	0.17336	3.41594	−0.06046	0.47179	4
YMnSb	−0.00442	2.94109	−0.02969	0.09358	3

3.4. Location associated with half-metallicity

In the experimental fabrication of HH alloys on a substrate to make device applications, lattice mismatch may happen due to the influence of various factors. For this "strain engineering" technique[35] is usually used to obtain the required electrical and physical properties of HH alloys through developing layered alloys by lattice mismatched substrates. Therefore, it is essential to further investigate the lattice parameter strain engineering by exploring the robustness belonging to the HM through changing the lattice constants of these two studied materials. Total magnetic moments and the spin moments of the Y, Cr, Mn, and Sb atom, with respect to lattice parameter are shown in the Fig. 8. When the lattice parameters of HH YCrSb and YMnSb materials are expanded, the hybridization between Y and Cr/Mn decreases, which leads to the rise in the spin moment of Cr/Mn and decrease in Y. The E_F found inside the gap and the number of majority spin states change a little in all these lattice variations. In addition, it is also observed that by varying the lattice constants in a wide range, there is slightly change in the overall total magnetic moment, and the overall total magnetic moments remain nearly 4 μ_B and 3 μ_B for YCrSb and YMnSb, respectively. It is also discovered that for the optimized equilibrium lattice constant for the stable X_I phase, the magnetic moments have integer values for both compounds, which is viewed as the character associated with HMF. Thus, these types of substrates may be handled as ideal applicants for the spintronic devices. Through the computations, the HM can be found to reach up to compression and expansion of −10.1% to 3.6% for YCrSB and for −12.3% to 2.7% for YMnSb. This verifies that magnetic properties can be tuned for these substrates by expanding and compressing their lattice parameters.

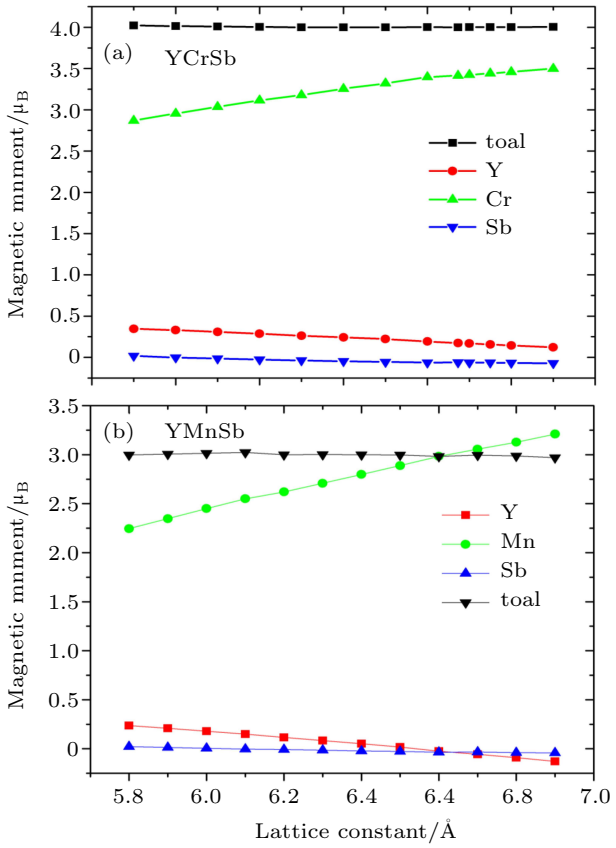


Fig. 8. (color online) Lattice parameter dependences of the total magnetic moment, and the spin moments of Y, Cr/Mn and Sb atoms for (a) YCrSb and (b) YMnSb, respectively.

4. Conclusions

In this work, structural, electronic, and magnetic properties of HH YCrSb and YMnSb materials with three different atomic arrangements (X_I, X_{II}, and X_{III}) are investigated by using FP–LAPW method. Calculated formation energies confirm that these compounds are chemically stable. Results revel that both YCrSb and YMnSb are true HMFs having integral magnetic moments of 4 μ_B and 3 μ_B, respectively. The total magnetic moments of the studied materials are mainly contributed by the Cr and Mn atoms respectively. The particular d–d hybridization between the transition-metal elements Y

and Cr/Mn sorts the semiconducting gap inside the majority-spin as some other transition-metal centered HH materials. We find that half-metallic gaps are 0.43 eV and 0.13 eV for the YCrSb and YMnSb HH compounds, respectively. The electronic structure and DOS calculations indicate that both YCrSb and YMnSb HH materials show semiconductor natures in majority spin channel and in contrast, conducting trend observed in minority spin channel. It is found that YCrSb and YMnSb preserve their HMs for lattice constant ranges of 5.77 Å–6.85 Å and 5.92 Å–6.81 Å, respectively and retain 100% spin polarization at the E_F.

Acknowledgment

Authors are thankful to the Higher Education Commission (HEC) of Pakistan for their financial support under research grant number 550/SRGP/R&D/HEC/2014.

References

[1] Bhat I H, Yousuf S, Bhat T M and Gupta D C 2015 *J. Magn. Magn. Mater.* **395** 81
[2] Umamaheswari R, Yogeswari M and Kalpana G 2014 *J. Magn. Magn. Mater.* **350** 167
[3] Huang W, Wang X, Chen X, Lu W, Damewood L and Fong C Y 2014 *Mater. Chem. Phys.* **148** 32
[4] De Groot R A, Mueller F M, Van Engen P G and Buschow K H J 1983 *Phys. Rev. Lett.* **50** 2024
[5] Ko V, Han G and Feng Y P 2010 *J. Magn. Magn. Mater.* **322** 2989
[6] Liu G D, Dai X F, Liu H Y, Chen J L, Li Y X, Xiao G and Wu G H 2008 *Phys. Rev. B* **77** 014424
[7] Chatterjee S, Singh V R, Deb A K, Giri S, De S K, Dasgupta I and Majumdar S 2010 *J. Magn. Magn. Mater.* **322** 102
[8] Alijani V, Winterlik J, Fecher G H, Naghavi S S and Felser C 2011 *Phys. Rev. B* **83** 184428
[9] Luo H, Liu G, Meng F, Wang L, Liu E, Wu G and Jiang C 2011 *Comput. Mater. Sci.* **50** 3119
[10] Jaiganesh G, Eithiraj R D and Kalpana G 2010 *Comput. Mater. Sci.* **49** 112
[11] Jedema F J, Filip A T and Van Wees B J 2001 *Nature* **410** 345
[12] Song W, Wang J and Wu Z 2009 *J. Chem. Phys.* **130** 114707
[13] Li J, Li Y, Dai X and Xu X 2009 *J. Magn. Magn. Mater.* **321** 365
[14] Soeya S, Hayakawa J, Takahashi H, Ito K, Yamamoto C, Kida A and Matsui M 2002 *Appl. Phys. Lett.* **80** 823
[15] Son Y W, Cohen M L and Louie S G 2006 *Nature* **444** 347
[16] Galanakis I and Mavropoulos P 2003 *Phys. Rev. B* **67** 104417
[17] Liu B G 2003 *Phys. Rev. B* **67** 172411
[18] Gao G Y, Yao K L, Şaşıoğlu E, Sandratskii L M, Liu Z L and Jiang J L 2007 *Phys. Rev. B* **75** 174442
[19] Dong S and Zhao H 2011 *Appl. Phys. Lett.* **98** 182501
[20] Ahmadian F and Alinajimi R 2013 *Comput. Mater. Sci.* **79** 345
[21] Perdew J P, Burke K and Ernzerhof M 1996 *Phys. Rev. Lett.* **77** 3865
[22] Kohn W and Sham L J 1966 *Phys. Rev.* **145** 561
[23] Andersen O K 1975 *Phys. Rev. B* **12** 3060
[24] Schwarz K, Blaha P and Madsen G K H 2002 *Comput. Phys. Commun.* **147** 71
[25] Jepson O and Anderson O K. 1971 *Solid State Commun.* **9** 1763
[26] Graf T, Felser C and Parkin S S 2011 *Prog. Solid State Chem.* **39** 1
[27] Helmholdt R B, De Groot R A, Mueller F M, Van Engen P G and Buschow K H J 1984 *J. Magn. Magn. Mater.* **43** 249
[28] Aliev F G 1991 *Physica B* **171** 199
[29] Ishida S, Masaki T, Fujii S and Asano S 1997 *Physica B* **239** 163
[30] Gruhn T 2010 *Phys. Rev. B* **82** 125210
[31] Umamaheswari R, Yogeswari M and Kalpana G 2013 *Solid State Commun.* **155** 62
[32] Murnaghan F D 1937 *Am. J. Math.* 235
[33] Huang W, Wang X, Chen X, Lu W, Damewood L and Fong C Y 2015 *J. Magn. Magn. Mater.* **377** 252
[34] Monir M E A, Khenata R, Baltache H, Murtaza G, Abu-Jafar M S, Bouhemadou A and Rached D 2015 *J. Magn. Magn. Mater.* **394** 404
[35] Lu H, Schaff W J, Hwang J, Wu H, Koley G and Eastman L F 2001 *Appl. Phys. Lett.* **79** 1489